Axial kinematic response of end-bearing piles to P waves

George Anoyatis [1, ¶], Raffaele Di Laora [2, §], George Mylonakis[1, *† ‡]

[1] *Department of Civil Engineering, University of Patras, Rio-26500, Greece*
[2] *Department of Civil Engineering, Second University of Naples, Via Roma 29, 81031 Aversa(CE), Italy*

SUMMARY

Kinematic pile-soil interaction under vertically impinging seismic P waves is revisited through a novel continuum elastodynamic solution of the Tajimi type. The proposed model simulates the steady-state kinematic response of a cylindrical end-bearing pile embedded in a homogeneous viscoelastic soil stratum over a rigid base, subjected to vertically-propagating harmonic compressional waves. Closed-form solutions are obtained for: (i) the displacement field in the soil and along the pile, (ii) the kinematic Winkler moduli (i.e., distributed springs and dashpots) along the pile, (iii) equivalent, depth-independent, Winkler moduli to match the motion at the pile head. The solution for displacements is expressed in terms of dimensionless transfer functions relating the motion of the pile head to the free-field surface motion and the rock motion. It is shown that: (a) a pile foundation may significantly alter (possibly amplify) the vertical seismic excitation transmitted to the base of a structure; and (b) Winkler moduli pertaining to kinematic loading differ from those for inertial loading. Simple approximate expressions for kinematic Winkler moduli are derived for use in applications.

KEY WORDS: kinematic interaction; piles; soil-structure interaction; vertical excitation; analytical solution; Winkler

1. INTRODUCTION

During earthquake shaking, structures supported on pile foundations are subjected to motions at the base which may deviate significantly from corresponding surface motions recorded at large distances from the structure. The resistance of piles to the impinging seismic waves in the absence of a superstructure results in a complex dynamic phenomenon referred in the literature to as kinematic interaction [1, 2, 3, 4, 5, 6, 7]. With reference to long piles in homogeneous soil, various studies [8, 9] have demonstrated that kinematic interaction might be insignificant in modifying lateral oscillations

*Correspondence to: George Mylonakis, Geotechnical Laboratory, Department of Civil Engineering, University of Patras, Rio-26500, Greece
†E-mail: mylo@upatras.gr
‡Associate Professor
§Post-Doctoral Associate
¶Ph.D. candidate

at the pile head and may, therefore, be neglected in design. On the other hand, during vertical oscillations piles tend to resist more effectively the imposed seismic displacements, thus resulting in significant modification (mostly reduction) of foundation motion even in homogeneous soil [10, 11, 12]. Despite structures are generally designed without consideration for vertical earthquake motions (since they are capable to carry vertical loads), there is evidence for a potentially detrimental role of the vertical component of earthquake excitation [12, 13]. Nevertheless, using the free-field soil motion as excitation may lead to significant overestimation of seismic actions and, therefore, to overly expensive designs. In this light, there is clearly a need for developing rational, yet simple and cost-effective design tools for estimating the effective motion exciting a structure supported on piles.

With reference to simple engineering approximations, the most efficient way of modeling dynamic pile-soil interaction is to replace the soil medium by a series of independent Winkler springs and dashpots, uniformly distributed along the pile axis [14, 15]. The substitution is convenient, as the multi-dimensional boundary value problem is reduced to that of a simple rod subjected to one-dimensional wave propagation in the vertical direction. The fundamental problem in the implementation of Winkler models lies in the assessment of the moduli of the Winkler springs and dashpots. It, therefore, appears that a rational model capable of providing dependable estimates of dynamic Winkler stiffness and damping to be used in engineering applications would be desirable. In the framework of linear elastodynamic theory, an approximate yet realistic analytical solution is presented in this paper for an axially loaded end-bearing pile in a homogeneous soil stratum. The model is based on a continuum solution pioneered by Tajimi [16] and later extended, among others, by Nogami & Novak [17], Saitoh [18] and Anoyatis & Mylonakis [19]. The soil is simulated as a hysteretic continuum, whereas the pile is treated as a rod in the realm of strength-of-materials theory. While maintaining conceptual and analytical simplicity, the proposed model has distinct advantages over other simple analytical models [20, 21, 12], as it is applicable at low frequencies, accounts for resonant phenomena and cut-off frequency effects, encompasses the continuity of the medium in the vertical direction and the compressibility of the soil material, and is free of empirical constants. Apart from its intrinsic theoretical interest, the study provides simplified expressions for static and dynamic Winkler moduli that can be used in design.

2. PROBLEM DEFINITION & MODEL DEVELOPMENT

The problem considered in this study is depicted in Figure 1: a single vertical pile of length L and solid circular cross section of radius d is embedded in a homogeneous soil stratum of thickness $H(=L)$, overlying a rigid base. The excitation consists of vertically impinging harmonic P waves, expressed through a time-varying displacement $u_g(t) = u_{g0}e^{i\omega t}$ of soil base, u_{g0} being the displacement amplitude and ω the cyclic excitation frequency. The pile is treated as an isotropic, linearly elastic rod of Young's modulus E_p and mass density ρ_p. The soil is modelled as a linearly viscoelastic continuum of mass density ρ_s, Poisson's ratio ν_s, and hysteretic damping β_s, expressed through a complex-valued shear modulus $G_s^* = G_s(1+2i\beta_s)$ and a constraint modulus $M_s^* = M_s(1 + 2i\beta_s)$. Pile-soil interface is considered perfectly bonded. It will be shown that the

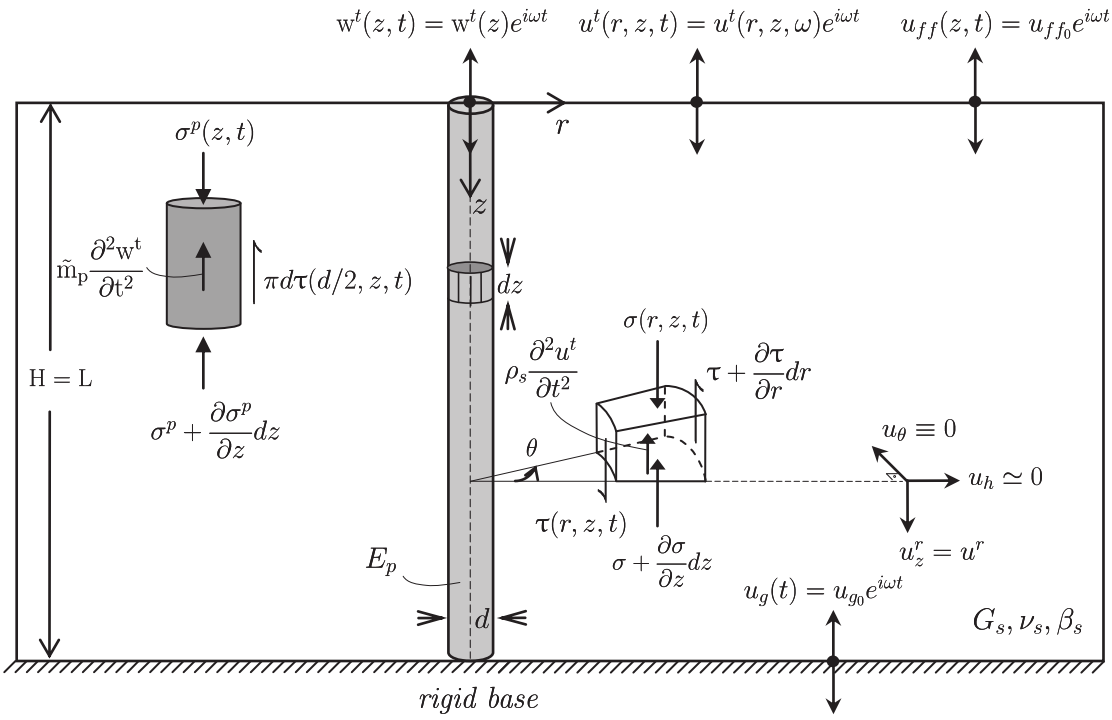

Figure 1. Problem considered

model, although idealized, provides valuable insight into the physics of kinematic response under vertically-propagating P waves.

2.1. Soil analysis

The equilibrium of forces in the vertical direction within the soil medium yields the differential equation [17, 19]

$$\frac{\partial(\tau\, r)}{\partial r} \;+\; r\,\frac{\partial \sigma}{\partial z} \;+\; r\,\rho_s\,\frac{\partial^2 u^t}{\partial t^2} \;=\; 0 \tag{1}$$

where $\tau = \tau_{rz}$ is the shear stress on θz plane, $\sigma = \sigma_z$ the normal stress on $r\theta$ plane, ρ_s the soil mass density and $u^t = u^t(r,z,t)$ the vertical soil displacement in an absolute (inertial) reference system. It is both conceptually and analytically convenient to express the soil motion relative to the motion of the rigid base u_g. Considering harmonic oscillations this can be expressed through the galilean transformation

$$u^t(r,z,\omega) \;=\; u^r(r,z,\omega) \;+\; u_{g_0} \tag{2}$$

Note that strains in the two reference systems coincide, as the spatial derivatives of the second term in the right-hand side of Equation (2) is zero. Fundamental to the proposed analysis is that the influence of the horizontal soil displacement component on the response is negligible ($u_h \simeq 0$) [17, 19]. As will be shown in the ensuing, this assumption is not particularly restrictive, as for the problem at hand, vertical displacement dominates over the corresponding horizontal

component close to the pile, and allows a direct uncoupling of the governing differential equations, which is not possible in classical elastodynamic theory [22]. Moreover, this physically-motivated simplification introduces a dimensionless compressibility parameter which relates propagation velocity of compressional waves in the soil medium, $V_p = \sqrt{M_s/\rho_s}$, to that of shear waves, $V_s = \sqrt{G_s/\rho_s}$, as $\eta_s = V_p/V_s$. A detailed discussion on the use of the specific material constant is provided in Reference [23]. For the problem at hand η_s is set equal to $\sqrt{2(1-\nu_s)/(1-2\nu_s)}$, stemming from the assumption $\varepsilon_r = \varepsilon_\theta = 0$ pertaining to the free-field condition.

In light of the above and with reference to the cylindrical coordinate system of Figure 1, the stress-displacement relations for τ and σ in Equation (1) are written in the approximate form:

$$\tau \simeq -G_s^* \frac{\partial u^r}{\partial r} \tag{3}$$

$$\sigma \simeq -\eta_s^2 G_s^* \frac{\partial u^r}{\partial z} \tag{4}$$

where η_s and G_s^* are the aforementioned compressibility parameter and complex soil shear modulus, respectively.

Substituting Equations (2), (4) and (3) into Equation (1), an uncoupled governing equation is obtained in the Fourier form

$$\frac{\partial^2 u^r}{\partial r^2} + \frac{1}{r}\frac{\partial u^r}{\partial r} + \eta^2 \frac{\partial^2 u^r}{\partial z^2} + \left(\frac{\omega}{V_s^*}\right)^2 u^r = -\left(\frac{\omega}{V_s^*}\right)^2 u_{g_0} \tag{5}$$

where $V_s^* = \sqrt{G_s^*/\rho_s}$ is the complex-valued propagation velocity of damped shear waves in the soil medium. Note that the above expression is identical to the one of the corresponding inertial interaction problem [17, 19], except from the non-homogeneous term in the right-hand side which stands for the effect of kinematic action.

According to standard analysis procedures for PDE's, the relative soil displacement u^r can be obtained as a superposition of a solution to the corresponding homogeneous equation expressed in terms of infinite trigonometric-Bessel series, and a particular solution associated with the non-homogeneous term in the right-hand side of Equation (5). Following References [17] and [24], the general solution to the homogeneous part of Equation (5) is

$$u_{hom}^r = [AI_0(qr) + BK_0(qr)]\,[C\sin az + D\cos az] \tag{6}$$

where A, B, C and D are integration constants to be determined from the boundary conditions.

To ensure bounded response at large distances from the pile ($r \to \infty$), constant A associated with the modified Bessel function of the first kind, $I_0()$, must vanish. Moreover, the traction-free condition at soil surface ($\partial u/\partial z = 0$) requires setting $C = 0$. The additional condition of zero relative displacement at rock level [$u^r(H) = 0$] yields the distinct values $a_m = (\pi/2H)(2m-1)$, $m = 1, 2, 3, ...$, stemming from the solution of the eigenvalue problem $\cos aH = 0$.

Accordingly, the relative soil displacement may be written in the form of the infinite trigonometric

sum

$$u^r(r,z,\omega) \;=\; \underbrace{\sum_{m=1}^{\infty} B_m\, K_0(q_m r)\, \cos a_m z}_{\text{homogenous solution}} \;+\; \underbrace{\sum_{m=1}^{\infty} U_m(r,\omega)\, \cos a_m z}_{\text{particular solution}} \tag{7}$$

where the remaining integration constant, B_m, has dimensions of length and can be determined from the compatibility condition at the pile-soil interface; $K_0()$ is the modified Bessel function of zero order and second kind, and q_m is the frequency-dependent wavenumber [19, 24]

$$q_m \;=\; \sqrt{(a_m \eta_s)^2 - \left(\frac{\omega}{V_s^*}\right)^2} \tag{8}$$

Note that the above expression relating q and a arises naturally from the application of separation of variables on the governing partial differential equation (Eq. 5). This results in a set of two ordinary differential equations, q and a being real positive integers pertaining to the modular ordinary differential equation with respect to the horizontal and vertical spatial variable r and z, respectively.

Function U_m in Equation (7) involves only the spatial coordinate r and can be established by substituting the particular solution into Equation (5). To this end, the forcing term in the right side of Equation (5) is expanded in Fourier series of the form $u_{g_0} \sum_{m=1}^{\infty} T_m\, (\omega/V_s^*)^2 \cos a_m z$, in the interval $0 \le z \le H$, to give

$$U_m(r,\omega) \;=\; \sum_{m=1}^{\infty} \left[Q_m\, K_0(q_m r) \;+\; T_m \left(\frac{\omega}{q_m V_s^*}\right)^2 u_{g_0} \right] \tag{9}$$

where Q_m is a new integration constant and

$$T_m \;=\; \frac{4\, \cos m\pi}{(1-2m)\pi} \tag{10}$$

is a modal participation coefficient corresponding to the expansion in Cosine series of the unit function.

Likewise, the vertical relative soil displacement and shear stress can be expressed, respectively, as

$$u^r(r,z,\omega) \;=\; \sum_{m=1}^{\infty} \left[B_m\, K_0(q_m r) + T_m \left(\frac{\omega}{q_m V_s^*}\right)^2 u_{g_0} \right] \cos a_m z \tag{11}$$

$$\tau(r,z,\omega) \;=\; G_s^* \sum_{m=1}^{\infty} B_m\, q_m\, K_1(q_m r)\, \cos a_m z \tag{12}$$

in which constant Q_m has been embodied into constant B_m.

2.2. Pile analysis

Considering the equilibrium of vertical forces acting upon an arbitrary pile segment modelled according to strength-of-materials theory, yields the differential equation

$$A_p \frac{\partial \sigma^p}{\partial z} + \pi\, d\, \tau(d/2, z, \omega) + \tilde{m}_p \frac{\partial^2 \mathrm{w}^t}{\partial t^2} = 0 \tag{13}$$

where σ^p is the vertical normal stress on the pile cross section, τ the vertical shear stress ("side friction") at the pile-soil interface in Equation (12), $\tilde{m}_p = \rho_p\, A_p$ the pile mass per unit pile length, ρ_p the pile material density and A_p the cross-sectional area. Following the previous developments, total vertical pile displacement w^t can be decomposed into base displacement u_g and pile displacement relative to base, w^r.

Considering harmonic oscillations of the form $\mathrm{w}(z,t) = \mathrm{w}(z)\, e^{i\omega t}$, one obtains

$$\mathrm{w}^t(z, \omega) = \mathrm{w}^r(z, \omega) + u_{g_0} \tag{14}$$

which is analogous to the corresponding decomposition for soil response in Equation (2).

Introducing stress-strain relations, the equation of motion of the pile is written in terms of displacements as:

$$E_p\, A_p \frac{\partial^2 \mathrm{w}^r}{\partial z^2} - \pi\, d\, \tau(d/2, z, \omega) + \omega^2 \tilde{m}_p\, \mathrm{w}^r = -\omega^2 \tilde{m}_p\, u_{g_0} \tag{15}$$

where E_p is the Young's modulus of the pile material. Similarly to Equation (5), the above expression differs from the one describing the corresponding inertial problem [17, 19] in the presence of the non-homogeneous term $-\omega^2 \tilde{m}_p\, u_{g_0}$ which accounts for kinematic action.
Assuming perfect contact at the pile-soil interface [i.e., $\mathrm{w}^r(z,\omega) = u^r(d/2, z, \omega)$], substituting Equations (11) and (12) into Equation (15) and employing the orthogonality conditions of the cosine functions in the interval $0 \le z \le H$, yields the frequency-dependent coefficient B_m

$$B_m = u_{g_0}\, b_m\, T_m \tag{16}$$

where b_m denotes the dimensionless constant

$$b_m = \frac{\dfrac{\omega^2\, \tilde{m}_p}{E_p\, A_p\, a_m^2} - \left(\dfrac{\omega}{q_m V_s^*}\right)\left[1 - \dfrac{\omega^2\, \tilde{m}_p}{E_p\, A_p\, a_m^2}\right]}{K_0(s_m)\left[1 - \dfrac{\omega^2\, \tilde{m}_p}{E_p\, A_p\, a_m^2}\right] + \dfrac{2\,\pi\, G_s^*\, s_m}{E_p\, A_p\, a_m^2}\, K_1(s_m)} \tag{17}$$

In light of the above analysis, the final expressions for relative displacements and shear stresses in the soil medium are

$$u^r(r,z,\omega) \;=\; u_{g_0} \sum_{m=1}^{\infty} \Big[b_m \, K_0(q_m r) + \Big(\frac{\omega}{q_m V_s^*} \Big)^2 \Big] \, T_m \, \cos a_m z \tag{18}$$

and

$$\tau(r,z,\omega) \;=\; u_{g_0} \, G_s^* \sum_{m=1}^{\infty} b_m \, q_m \, K_1(q_m r) \, \Big(\frac{\omega}{q_m V_s^*} \Big)^2 \, T_m \, \cos a_m z \tag{19}$$

Systematic verification studies and comparisons against results from rigorous numerical solutions reported below, confirm the validity of the above analysis.

The role of boundary conditions in the proposed formulation is worth discussing. To this end, a careful examination of the solution reveals that the boundary conditions in the pile and the soil coincide through the compatibility of deformations at the interface [i.e., $\mathrm{w}^r(z,\omega) = u^r(d/2,z,\omega)$], as do the equations of motion (homogeneous parts of Equations 5 and 15). Consequently, the natural modes expressed by eigenfunctions $\cos a_m z$ are identical in the two media which, in turn, allow the coefficients B_m to be obtained in closed form through Equations 16 and 17. Any deviation from the above conditions, such as in the case of a floating pile experiencing a finite amount of displacement at the tip, a non-uniform pile or an inhomogeneous soil layer, will result in a different set of eigenfunctions for the pile and the soil media, which will yield an infinite set of simultaneous algebraic equations for coefficients B_m, to be solved numerically. This variant of the method lies beyond the scope of this work and is explained by Anoyatis & Mylonakis [25] and Younan & Veletsos [26] for the analysis of related pile and retaining wall problems, respectively. A numerical investigation conducted by the authors (not shown in the interest) indicated that H/L ratio is not dominant for floating piles, whose kinematic response may approach that end-bearing piles for long piles (high L/d) and soft soil (low E_p/E_s).

The results discussed in the ensuing are presented in terms of the dimensionless frequency ratio ω/ω_1, ω_1 being the fundamental natural frequency of the soil layer in compression-extension. Note that the sequence of resonant soil frequencies can be readily determined from the familiar relation [27, 28]:

$$\omega_m \;=\; \frac{\pi V_p}{2H}(2m-1), \quad m = 1,2,3,... \tag{20}$$

For $m=1$ the above equation yields the classical result $\omega_1 = (\pi/2)/(V_p/H)$, corresponding to the dimensionless frequency parameter $\mathrm{a}_{0,1} = \omega_1 d/V_p = (\pi/2)/(H/d)^{-1}$, $\mathrm{a}_0 = \omega d/V_s$ being the familiar dimensionless frequency [23]. This frequency is often referred to as "cutoff frequency" (a_{cutoff}), as only for dimensionless frequencies a_0 above $\mathrm{a}_{0,1}$ (or, equivalently, cyclic frequencies above ω_1) stress waves can propagate horizontally in the soil medium. Obviously, this wave field develops in addition to the standing wave field produced by the up- and down- propagating waves in the free-field soil and is, thereby, referred to as "scattered wave field" [1].

In the following, the accuracy of the proposed analytical model is validated through comparisons against results from rigorous Finite-Element (FE) analyses, performed using the commercial computer platform ANSYS [29]. To this end, 4-noded axisymmetric elements were employed to

model the soil and the pile. The lateral dimension of the model was set in the range $10^2 - 10^3\, d$, to ensure that soil response close to the boundaries is not affected by the outward-spreading scattered waves even at the lowest damping ratio considered ($\beta_s = 5\%$). Radial displacements were restrained along the lateral boundary of the mesh to simulate one-dimensional P-waves at large distances from the pile. Likewise, nodes at the base of the model were fully restrained to account for the presence of rigid bedrock. Soil elements of constant vertical thickness equal to $d/2$ and horizontal length of $d/8$ at the pile-soil interface, increasing with radial distance up to $3\,d/2$ close to the lateral boundary, were employed. The analysis was carried out in the frequency domain employing hysteretic damping in the soil, as in the analytical model.

Moreover, results from the proposed model are compared to corresponding results obtained from the kinematic Winkler model in Reference [12]. The spring and dashpot coefficients employed in that study are based on inertial interaction analyses, following the early work of Roesset [30] and Gazetas & Dobry [31]:

$$k \;=\; 0.6E_s\Big(1+\frac{1}{2}\sqrt{\mathrm{a}_0}\Big), \qquad \beta \;=\; \frac{\pi}{2}\,\frac{\eta_s}{(1+\nu_s)}\,\frac{\mathrm{a}_0^{3/4}}{1+0.5\sqrt{\mathrm{a}_0}} \;+\; \beta_s \tag{21a,b}$$

In the ensuing, the Fourier series are evaluated using 10^3 terms; ν_s is taken equal to 0.4 and ρ_s/ρ_p equal to 0.7.

3. KINEMATIC RESPONSE & AMPLIFICATION FACTORS

As explained in the foregoing, the vertically propagating P-waves in the soil are diffracted/scattered by the stiffer pile, thereby modifying the wave field, with the vertical displacement atop the pile $\mathrm{w}_0^t(\omega)$ differing from the free-field surface displacement $u_{ff_0}(\omega)$. To quantify this deviation a kinematic response factor I_v is introduced as the ratio of absolute motions (displacements, velocities, accelerations) at the pile head and the free-field surface i.e.,

$$I_\mathrm{v} \;\equiv\; \frac{\mathrm{w}_0^t(\omega)}{u_{ff_0}(\omega)} \;=\; \frac{1 \;+\; \displaystyle\sum_{m=1}^{\infty}\Big[b_m\,K_0(s_m) + \Big(\frac{\omega}{q_m V_s^*}\Big)^2\Big]T_m}{1 \;+\; \displaystyle\sum_{m=1}^{\infty}\Big(\frac{\omega}{q_m V_s^*}\Big)^2 T_m} \tag{22}$$

where b_m is provided by Equations (17); $s_m = q_m d/2$ is given by

$$s_m \;=\; \mathrm{a}_{cutoff}\,\frac{\eta}{2}\sqrt{(2m-1)^2 - \frac{(\mathrm{a}_0/\mathrm{a}_{cutoff})^2}{1+2i\beta_s}} \tag{23}$$

where $(\mathrm{a}_0/\mathrm{a}_{cutoff})$ can be interpreted as (ω/ω_1).

The profile of the free-field motion with depth can be easily determined from Equation (18) by letting $r \to \infty$ to give

$$u_{ff}(z,\omega) \;=\; u^t(r\to\infty,z,\omega) \;=\; u_{g_0}\left[1 \;+\; \sum_{m=1}^{\infty}\left(\frac{\omega}{q_m V_s^*}\right)^2 T_m \;\cos\alpha_m z\right] \tag{24}$$

which provides an alternative representation of the familiar solution [27, 28]

$$u_{ff}(z,\omega) \;=\; u_{g_0}\,\frac{\cos\left(\dfrac{\omega z}{V_p^*}\right)}{\cos\left(\dfrac{\omega H}{V_p^*}\right)} \tag{25}$$

The variation of $|I_{\rm v}|$ with frequency is explored in Figures 2 and 3, for soil material damping $\beta_s =$ 0.05 and 0.10, respectively. The predictions of the proposed model (Equation (22)) are compared to results obtained from the kinematic Winkler model in Reference [12] and a rigorous FE solution [29] for a large set of pile-soil configurations and frequencies. Evidently, the proposed continuum solution is in better agreement with the FE results than the Winkler model.

As expected, at zero frequency $|I_{\rm v}|$ is equal to unity, which indicates that the pile follows long wavelengths in the soil. As a general trend, $|I_{\rm v}|$ fluctuates with increasing frequency attaining values lower than unity. For short and/or stiff piles ((a), (d), (e), (f) in Figures 2 and 3) minima occur at the natural frequencies of the soil layer, where the free-field response (denominator in Equation (22)) maximizes, thus lowering factor $|I_{\rm v}|$. An extreme case is represented by an infinitely stiff pile ($\mathrm{w}_0^t = u_{g_0}$) for which $I_{\rm v}$ is clearly equal to $\cos(\omega H/V_p^*)$. All methods capture this behavior and provide identical results for both very stiff and very short piles (Figures 2(d), 3(d)). These fluctuations are suppressed for long piles and low pile-soil stiffness ratios (Figures 2(c), 3(c)). However, for short piles and high pile-soil stiffness ratios, $|I_{\rm v}|$ may exceed unity in the high frequency range which indicates that the pile head moves more than the free-field soil surface (Figure 2(d)). The amplification of motion is more pronounced for higher soil material damping, as shown in Figures 3 (a), (d), (e). This can be explained given that higher values of β_s tend to suppress soil response, whereas pile response is less sensitive to soil damping, thus leading to an increase in $|I_{\rm v}|$. Moreover, it is observed that at $\omega = \omega_1$ the proposed solution underestimates $|I_{\rm v}|$ whereas the Winkler model overestimates pile motion compared to the rigorous FE results. The less satisfactory performance of both analytical models at low values of pile-soil stiffness ratio ($E_p/E_s = 100$) may be attributed to their inability to capture the effect of radial response of the pile, which, naturally, plays an increasingly important role as the stiffness contrast between pile and soil decreases. This, however, is of minor importance in most cases of practical interest. The less satisfactory predictions of the Winkler model may also be attributed to the sensitivity of the results on the selection of the Winkler parameters.

Figures 2 and 3 show that the axial kinematic response of a single pile is governed by the combined effect of pile slenderness and pile-soil stiffness ratio, as the kinematic response factor of several different pile-soil configurations seem to follow the same trend (e.g., Figures 2(a) and 2(f)). This can be analytically braced through the dimensionless parameter λL, where $\lambda = (k/E_p A_p)^{1/2}$

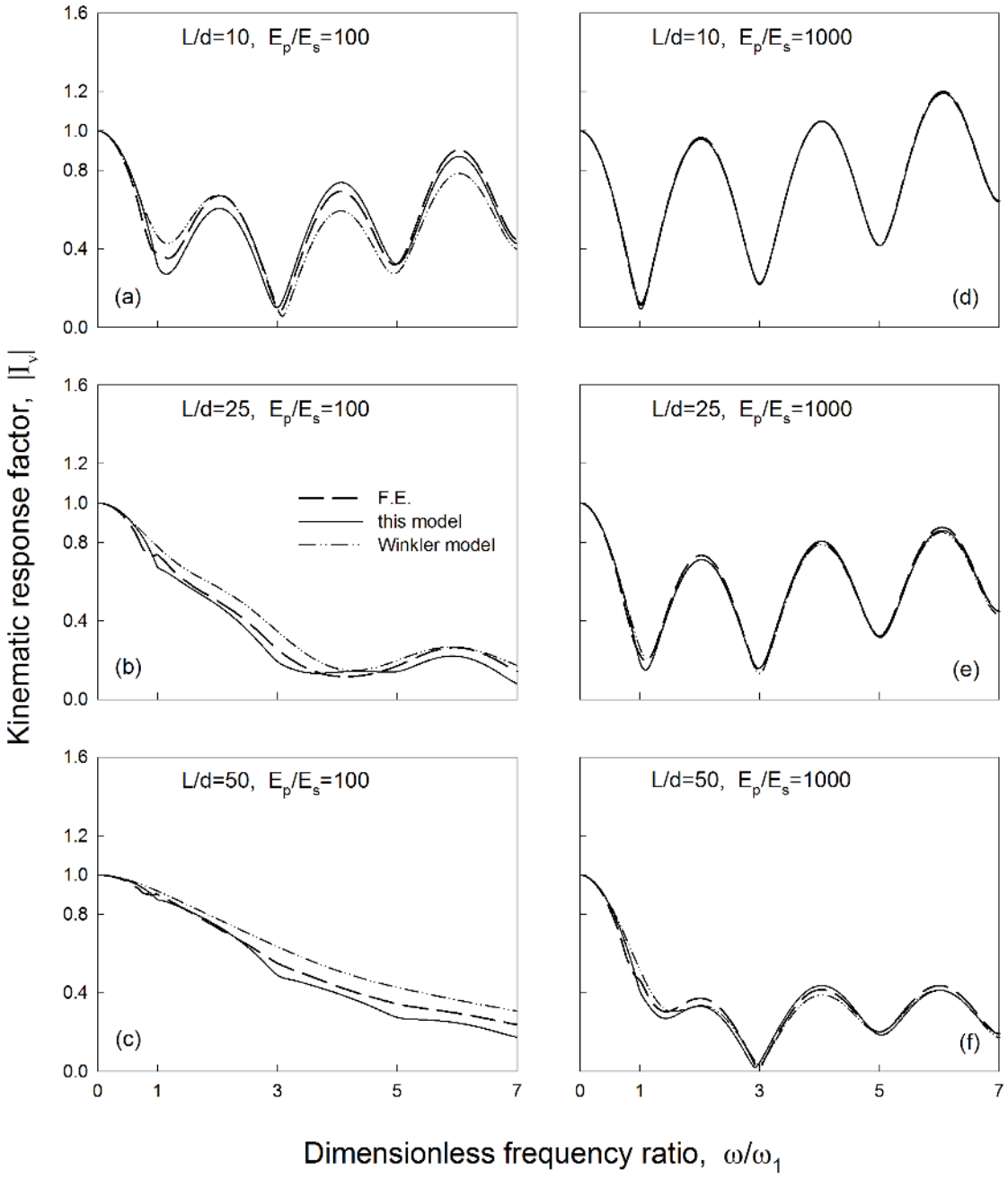

Figure 2. Variation of kinematic response factor I_{v} with frequency. Comparison of predictions of the proposed analysis against results from rigorous FE and Winkler formulations; $\beta_s = 0.05$

is a characteristic wavenumber, k the spring stiffness and L the pile length. In Winkler analyses, λL is a dimensionless slenderness parameter controlling pile response. In the same token, in continuum models $L_m = (L/d)(E_p/E_s)^{-1/2}$ may be viewed as a *mechanical* slenderness ([33]) which, like λL, encompasses geometrical slenderness and pile-soil stiffness ratio. Evidently, pile-soil systems characterized by similar values of mechanical slenderness L_m, tend to behave in a similar way.

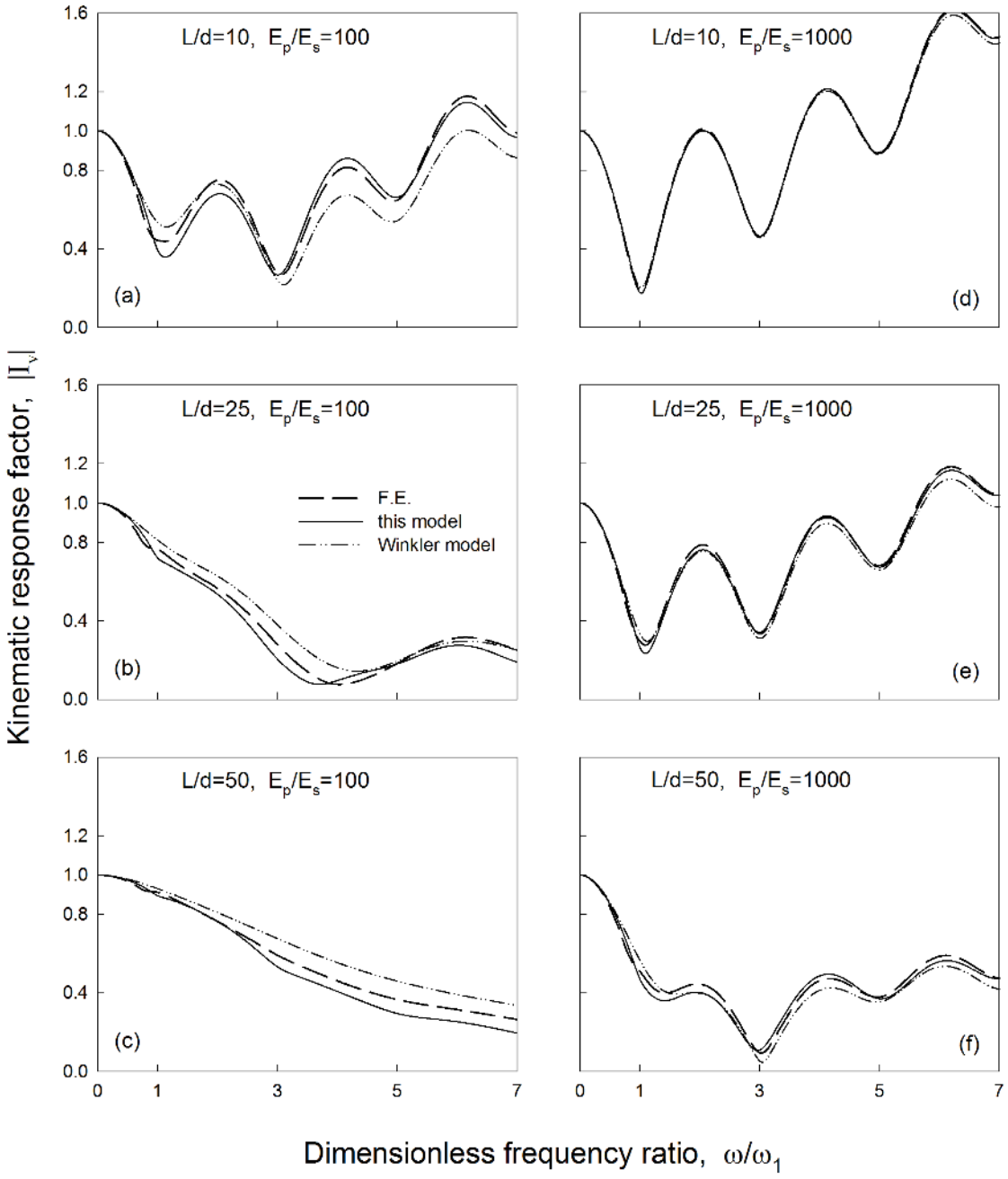

Figure 3. Variation of kinematic response factor I_{v} with frequency. Comparison of predictions of the proposed analysis against results from rigorous FE and Winkler formulations; $\beta_s = 0.10$

In addition to the kinematic response factor I_{v}, a kinematic amplification factor A can be introduced as the ratio of displacement at the pile head over the prescribed displacement at the base i.e.,

$$\mathsf{A} \equiv \frac{\mathrm{w}_0^t(\omega)}{u_{g_0}(\omega)} = 1 + \sum_{m=1}^{\infty} \left[b_m \, K_0(s_m) + \left(\frac{\omega}{q_m V_s^*} \right)^2 \right] T_m \tag{26}$$

The variation of |A| with frequency is depicted in Figure 4. As a general trend, the maximum amplification in terms of |A| is observed at first resonance. Higher values of pile slenderness L/d correspond to higher maxima. Also, an increase in soil material damping and pile-soil stiffness ratio suppresses the amplification of motion at pile top, the first controlling free-field response and the latter increasing soil-structure interaction. Overall, the results seem to indicate that significant amplification may occur only close to first resonance.

Comparing results in terms of A and I_{v}, it is noted that $|I_{\mathrm{v}}|$ may exceed unity for stiff piles ($L_m < 1$) at certain frequencies whereas corresponding |A| values are less than 1. This suggests that pile motion is of higher amplitude than surface soil motion away from the pile, which, however, is lower than base motion due to soil deamplification at frequencies $\omega_n = (n\pi V_p)/H$, with $n = 1, 2, 3, etc.$.

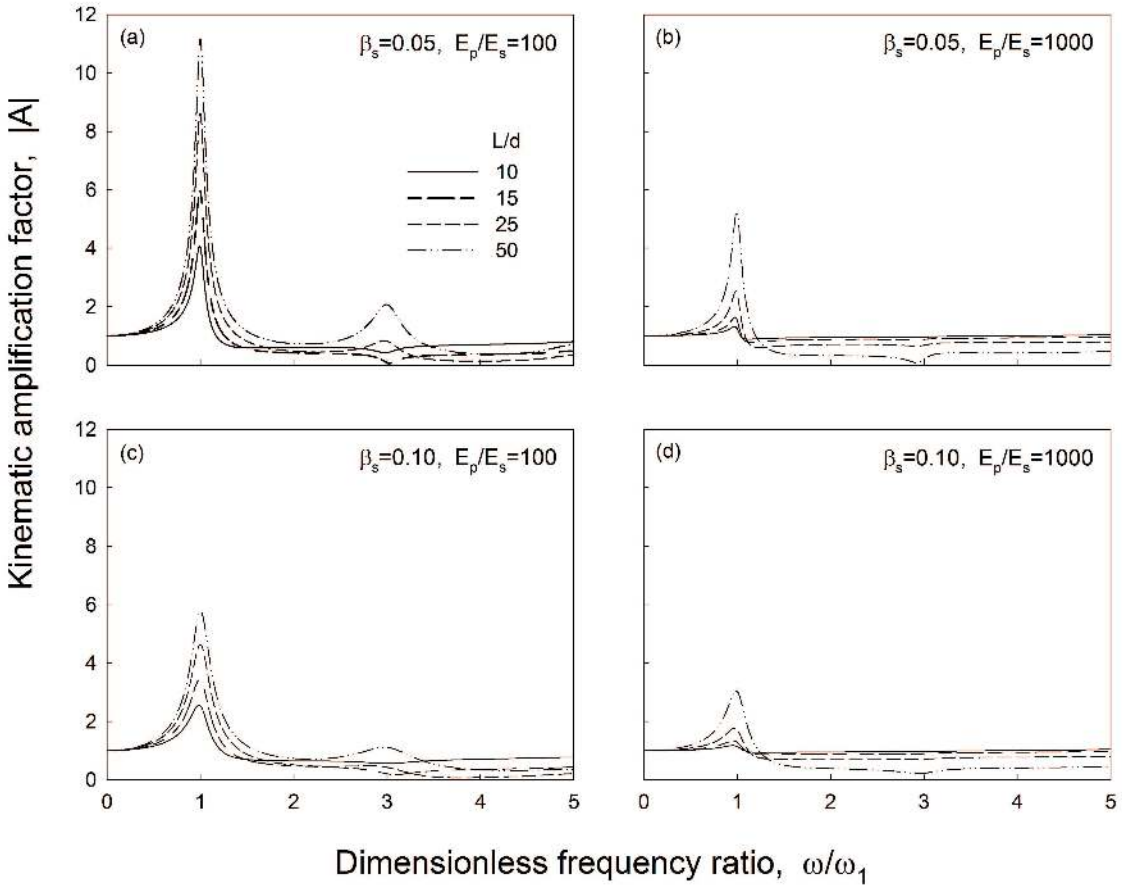

Figure 4. Variation of kinematic amplification factor A with frequency for different pile-soil configurations.

4. ACTUAL (DEPTH-DEPENDENT) KINEMATIC WINKLER MODULUS

Dynamic Winkler modulus along the pile can be defined according to the proposed solution, by dividing the vertical soil reaction at the pile-soil interface and the corresponding relative

displacement between pile and free-field soil for each frequency ω at depth z

$$k^*(z,\omega) \;\equiv\; \frac{\pi\, d\, \tau(d/2,z,\omega)}{\mathrm{w}^t(z,\omega) \;-\; u_{ff}(z,\omega)} \tag{27}$$

The above modulus is both complex-valued and depth-dependent, and can be cast in the convenient form $k^* = k(1+2i\beta)$. The real part of k^* represents the dynamic stiffness of the Winkler spring k and the imaginary part over twice the real part stands for an effective damping coefficient β, which encompasses both hysteretic (β_s) and radiation (β_r) energy dissipation in the soil surrounding the pile [17, 19].
On the basis of Equation (27), the Winkler modulus is obtained as

$$k^*(z,\omega) \;=\; 2\,\pi\, G_s^* \,\frac{\displaystyle\sum_{m=1}^{\infty} b_m\; s_m\; K_1(s_m)\,\left(\frac{\omega}{q_m V_s^*}\right)^2 T_m\;\cos a_m z}{\displaystyle\sum_{m=1}^{\infty} b_m\; K_0(s_m)\, T_m\;\cos a_m z} \tag{28}$$

4.1. Static behavior

In principle, purely static Winkler moduli for kinematic loading cannot be defined, as at $\omega = 0$ no relative displacements between pile and soil can develop and, therefore, no vertical shear stresses can exist at the pile-soil interface. Accordingly, the static value of Winkler modulus can be investigated only in the limit sense, by setting $\beta_s = 0$ and letting $\omega \to 0$ in Equation (28).

The variation of static k with depth is presented in Figure 5 for selected values of pile slenderness. The proposed results (thick curves) are compared to those obtained from the corresponding inertial modulus (thin curves) referring to a pile subjected to a static axial load at the head [17, 23, 19]. It is shown that kinematic Winkler modulus increases monotonically with depth, the increase being stronger close to the rigid base. Owing to the fixed boundary condition at $z = L$, both numerator and denominator in Equation (28) tend to zero, with the latter approaching the limit value at a higher rate, leading to an infinite ratio (modulus k) at the tip. As in inertial interaction, soft and slender piles produce lower k values than corresponding squatty and stiff piles. It is also observed that the corresponding modulus for inertial interaction follows a similar trend in an inverse manner, yet attains lower values. This difference may be attributed to the different excitation sources in the two configurations.

The lack of dependence of soil material damping on frequency in the above analysis will invariably lead to a Winkler modulus at $\omega \to 0$ that will slightly deviate from the corresponding static counterpart in a damped medium. To overcome the problem, the expression for complex shear modulus $G_s^* = G_s(1+2i\beta_s)$ can be replaced by

$$G_s^* \;=\; G_s[1 + 2i\beta_s f(\omega)] \tag{29}$$

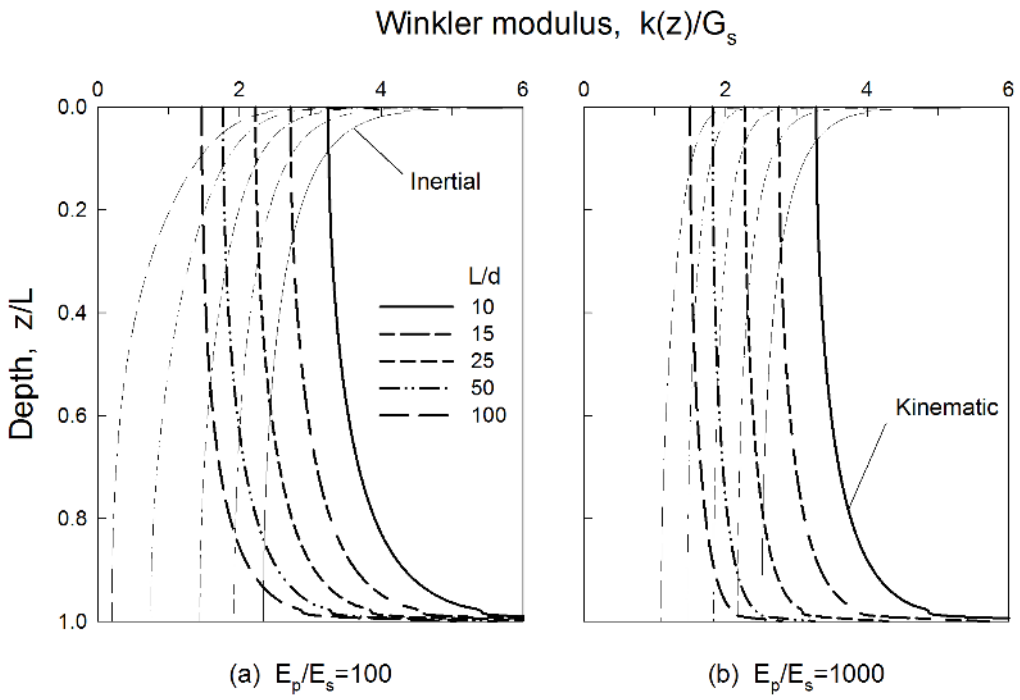

Figure 5. Kinematic vs inertial Winkler modulus with depth for static conditions ($\omega = 0$).

where

$$f(\omega) \;=\; \frac{2}{\pi}\,\tanh[\varepsilon^{-1}\,(\omega/\omega_1)] \tag{30}$$

is a real-valued dimensionless function of frequency in which ω_1 is the fundamental natural frequency of the soil layer and ε is a pertinent penalty parameter (typically varying between 10^{-3} to 10^{-4} [34]). Evidently, the above formulation forces the dynamic solution to converge to the static value at $\omega \to 0$. Moreover, its odd nature [i.e., $f(-\omega) = -f(+\omega)$] allows for direct application of the solution in discrete Fourier transform procedures for transient loads ([35]). Note that this correction does not address the issue of causality which can be treated by other procedures ([36]). Both issues are of minor importance from a practical viewpoint and will not be further discussed in this work.

4.2. Dynamic behavior

The variation of dynamic Winkler moduli with depth is provided in Figure 6 for different values of excitation frequency and pile-soil stiffness ratio. For $\omega \to 0$, the dynamic spring stiffness follows a monotonic increase with depth, which is stronger for soft piles ($E_p/E_s = 100$) and is practically equal to the static case. On the other hand, low-frequency damping coefficient β is independent of depth and pile-soil stiffness ratio, and is equal to soil material damping. This is anticipated since for frequencies below the fundamental natural frequency of the system (cutoff frequency) diffracted waves cannot propagate (horizontally) in the soil and thus no radiation damping can be generated. At $\omega = \omega_1$ the trend is reversed, as a monotonic increase of β is observed, while dynamic k is

constant with depth. At high frequencies ($\omega > 3\omega_1$) both damping and stiffness moduli experience fluctuations with depth, which are stronger for stiff piles ($E_p/E_s = 1000$) and, hence, no monotonic trend develops.

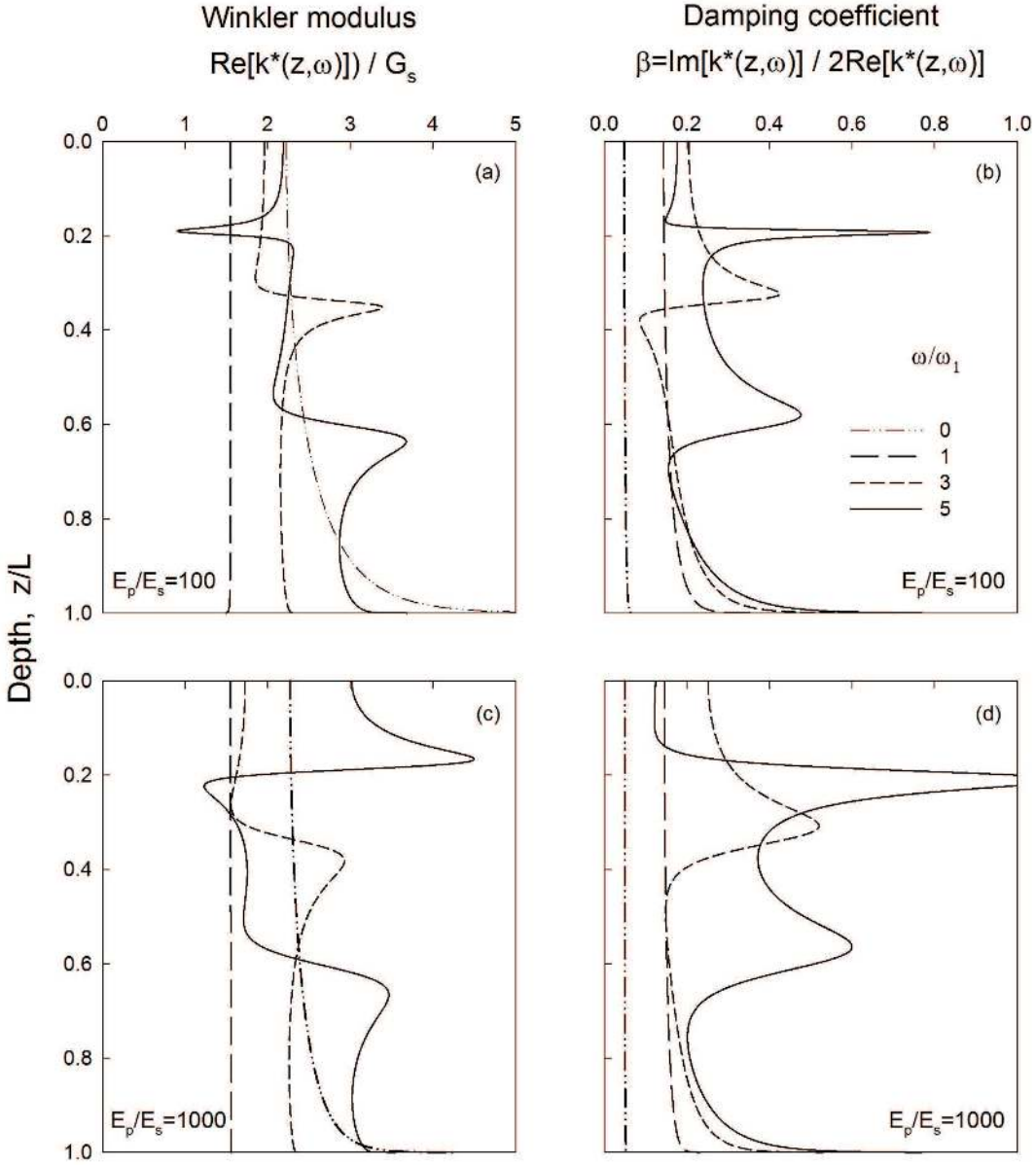

Figure 6. Variation of dynamic Winkler modulus with depth for different pile-soil configurations; $L/d = 25$, $\beta_s = 0.05$.

The variation of kinematic Winkler moduli k and β with depth for frequencies up to cutoff ($0 \leq \omega \leq \omega_1$) is further investigated in Figures 7 and 8, respectively. In Figure 7 a common trend is noticeable: with increasing frequency spring stiffness drops and gradually becomes less sensitive to both depth and pile-soil stiffness ratio. At $\omega = \omega_1$, k is essentially independent of z, depending solely on pile slenderness, with lower L/d's generating higher k's. This occurs only at first resonance and indicates the development of plane strain conditions in the domain. Interestingly, this

behavior does not develop for coefficient β (Figure 8), which decreases with decreasing frequency and gradually becomes essentially independent of depth and pile-soil stiffness ratio. In addition, at $\omega = 0$ β is independent of L/d, being merely equal to soil material damping β_s. Finally, the influence of E_p/E_s on k and β becomes significant close to the pile tip and is more pronounced for slender piles especially at high frequencies.

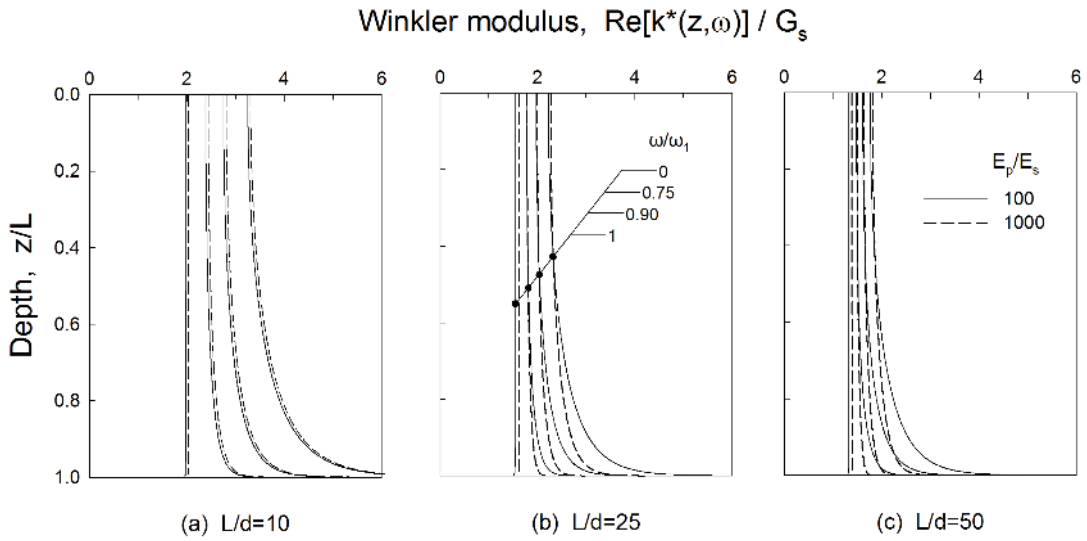

Figure 7. Variation of Winkler modulus with depth for different frequencies and pile-soil configurations; $\beta_s = 0.05$.

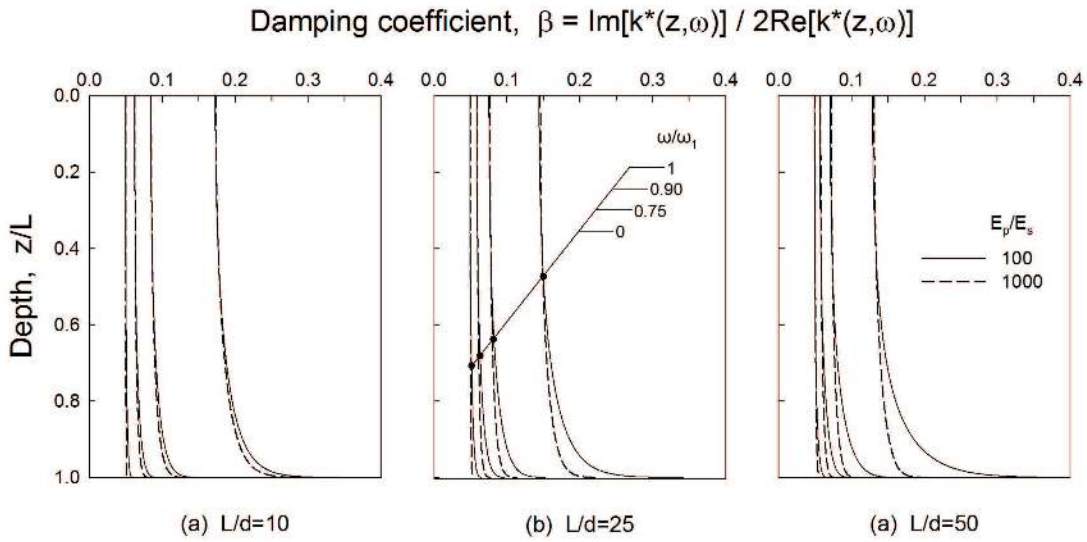

Figure 8. Variation of damping coefficient with depth for different frequencies and pile-soil configurations; $\beta_s = 0.05$.

5. AVERAGE (DEPTH-INDEPENDENT) KINEMATIC WINKLER MODULUS

The above analysis reveals that the distribution of Winkler moduli along the pile depend on depth even in homogeneous soil. Yet this type of modeling is difficult to be implemented in routine engineering procedures, as it leads to differential equations with variable coefficients. An easier alternative can be developed by means of equivalent, depth-independent, moduli which can be obtained by equating the kinematic response factor $I_{\rm v}$ to that derived from a Winkler model based on constant springs and dashpots with depth.

To this end, a candidate solution is that in Reference [12], expressed by

$$I_{\rm v} \;=\; (1-\Theta)\,\frac{\cos(\omega H/V_p^*)}{\cosh \lambda H} \;+\; \Theta \tag{31}$$

where

$$\Theta \;=\; \frac{k^*}{E_p\,A_p\left[(\omega/V_p^*)^2+\lambda^2\right]}, \qquad\qquad \lambda \;=\; \sqrt{\frac{k^*-\omega^2\tilde{m}_p}{E_p\,A_p}} \tag{32a,b}$$

stand for a dimensionless coefficient and a Winkler parameter with dimensions $[L^{-1}]$, respectively. Given the transcendental nature of the above equations, the solution can be obtained iteratively by equating the real and imaginary parts of $I_{\rm v}$ in Equations (22) and (31).

Results from the above procedure are presented in Figures 9 and 10. The variation of average Winkler moduli with frequency is plotted in Figure 9 for a family of soft ($E_p/E_s = 100$) and stiff ($E_p/E_s = 1000$) piles with slenderness $L/d = 25$ and different soil material damping. Due to the existence of a sequence of resonant frequencies in compression-extension (provided by Equation (20)), no monotonic trend is evident in the results. The first resonance or cutoff frequency is inherently associated with the emergence of horizontally propagating ("diffracted") waves in the soil around the pile. For frequencies up to this threshold value ($0 \le \omega \le \omega_1$), the stiffness of Winkler springs decreases with frequency and is practically independent of soil material damping (Figure 9(a), (c)), whereas damping coefficient β is practically equal to soil material damping β_s (Figure 9(b), (d)). At cutoff frequency ($\omega = \omega_1$) stiffness k drops to a minimum, the drop being smaller for higher values of β_s and becomes zero for an undamped soil ($\beta_s = 0$). Effective damping β exhibits a jump due to the sudden emergence of wave radiation in the medium.

The variation of Winkler moduli with frequency for selected values of pile slenderness and two values of pile-soil stiffness ratio is presented in Figure 10 for soil material damping $\beta_s = 0.05$. As a general trend, higher values of k correspond always to lower values of L/d (Figures 10(a), 10(d)), whereas the opposite is true for the damping coefficient (Figures 10(c), 10(d)). Note that this pattern is not valid for frequencies beyond second resonance ($\omega > 3\omega_1$).

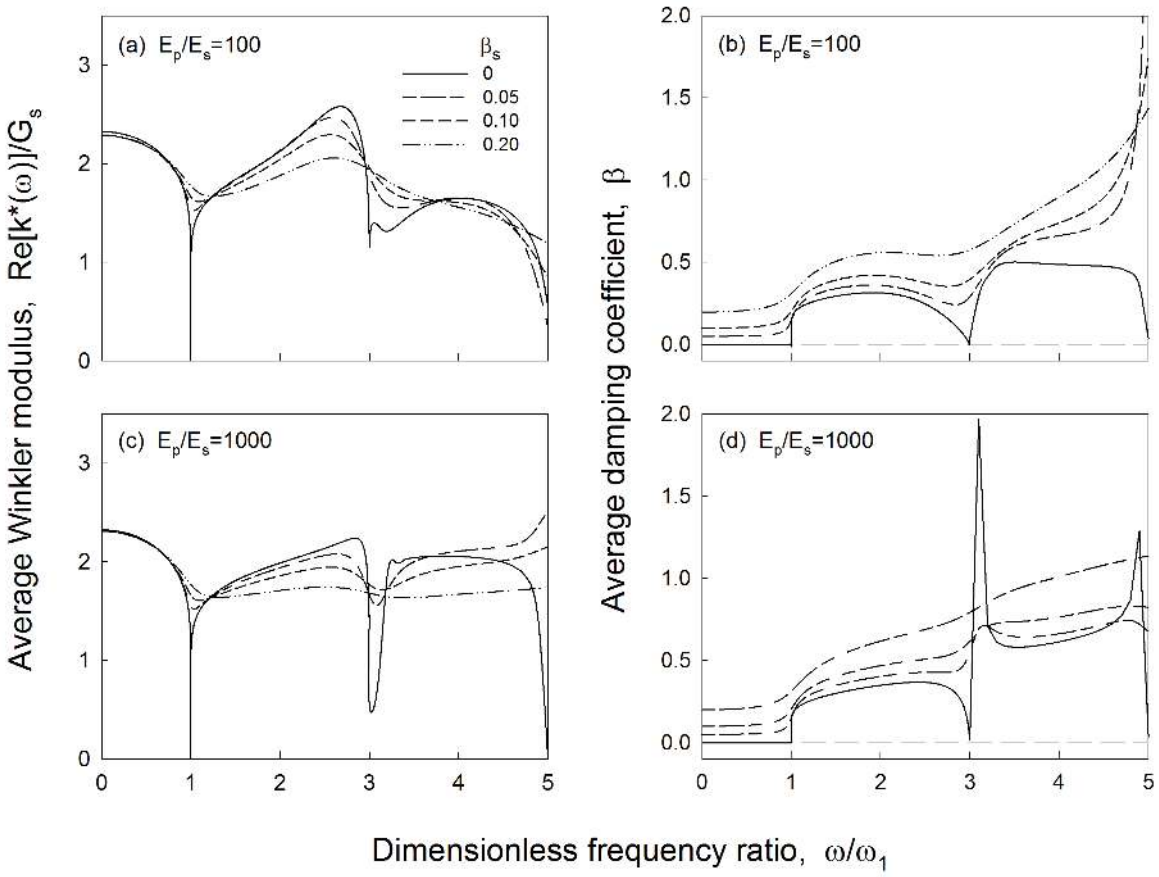

Figure 9. Variation of depth-independent Winkler moduli with frequency for various pile-soil configurations; $L/d = 25$.

6. SIMPLE FORMULAE

The average Winkler moduli presented above may be well approximated by a variant of the plane strain model of Baranov [20] and Novak [21] given by the familiar equation

$$k^*(\omega) \;=\; 2\,\pi\,G_s^*\,s\,\frac{K_1(s)}{K_0(s)} \tag{33}$$

where $K_1()$ and $K_0()$ are the modified Bessel functions of the second kind and zero and first order, respectively, and s is a complex-valued dimensionless parameter. Contrary to the plane strain model where the argument s is equal to $\mathrm{a}_0/\sqrt{1+2i\beta_s}$, leading to a solution that does not account for resonant effects, in the proposed simplified formulation s is given by

$$s \;=\; \mathrm{a}_{cutoff}\,\frac{\eta_s}{2}\,\sqrt{1-\frac{(\mathrm{a}_0/\mathrm{a}_{cutoff})^2}{1+2i\beta_s}}, \qquad \mathrm{a}_{cutoff}=\frac{\omega_1 d}{V_p}=\frac{\pi}{2}\Big(\frac{H}{d}\Big)^{-1}, \qquad \eta=\sqrt{\frac{2(1-\nu_s)}{1-2\nu_s}} \tag{34a,b,c}$$

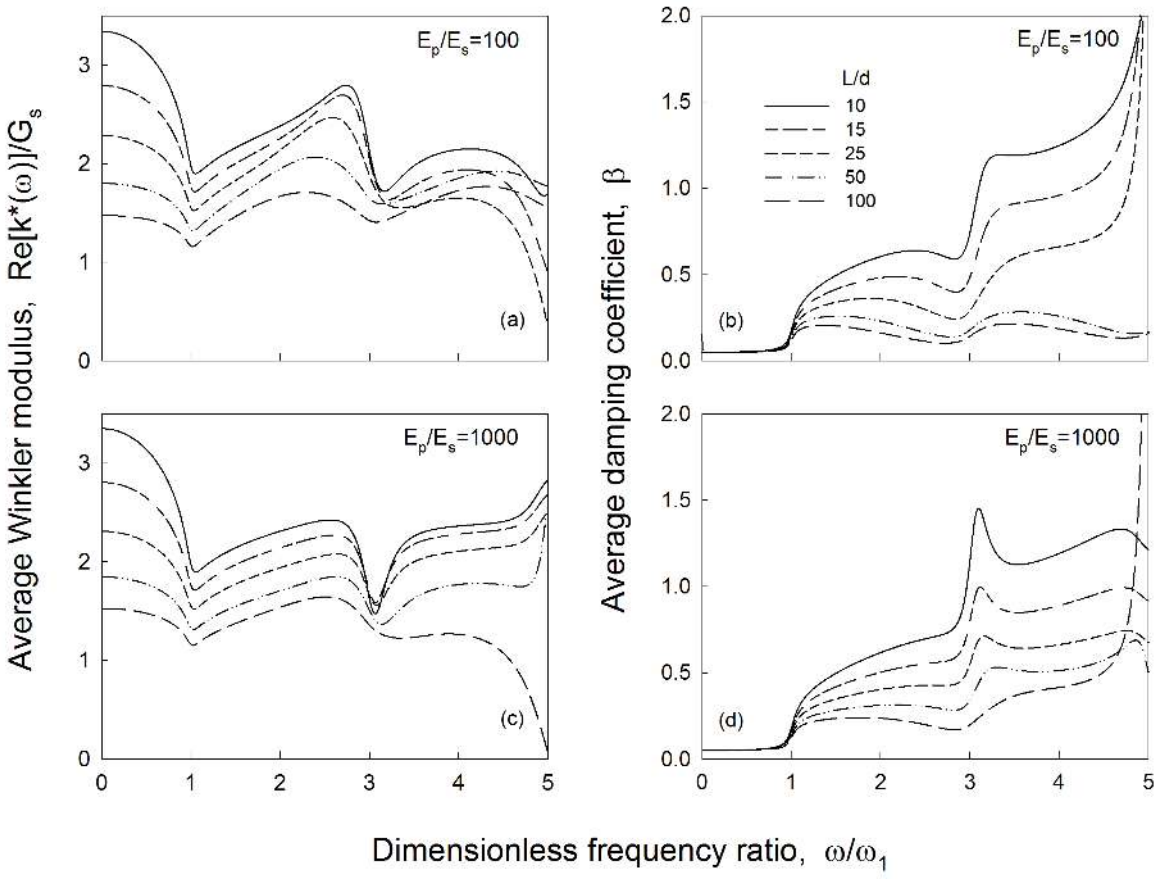

Figure 10. Variation of depth-independent Winkler moduli with frequency for various pile-soil configurations; $\beta_s = 0.05$.

which can be obtained from the full solution in Equation (23) by setting $m = 1$. Results from this analysis are compared in Figure 11 to those obtained from the proposed solution in Section 5. It is noted that values from Equation (33) are much closer to the actual values compared to those arising from the formulation in Reference [12], which do not account for cutoff frequency and pile slenderness. Following References [32] and [19], an approximation to the above solution can be obtained by means of the formula

$$k^*(\omega) \;=\; \left[\frac{2\,\pi\,(1+2i\beta_s)}{\ln(2/s)-\gamma} \;+\; (\mathrm{a}_0^2 - \mathrm{a}_{cutoff}^2)\,(1+i/2)\right] G_s \tag{35}$$

which is based on power series (McLaurin) expansion of parameter s around zero. In the above expression, γ denotes Euler's number ($\simeq 0.577$).

Equations (33) and (35) can be employed to approximate Winkler modulus for both inertial and kinematic loading. The difference between the two cases lies in the use of a different compressibility coefficient η (see Equation (34c) and Reference [19]). Note that in the present study, Equation (33) is nearly exact at resonance ($\omega = \omega_1$), leading to a true depth-independent modulus - a consequence of the dominant role of the first resonant mode on the response.

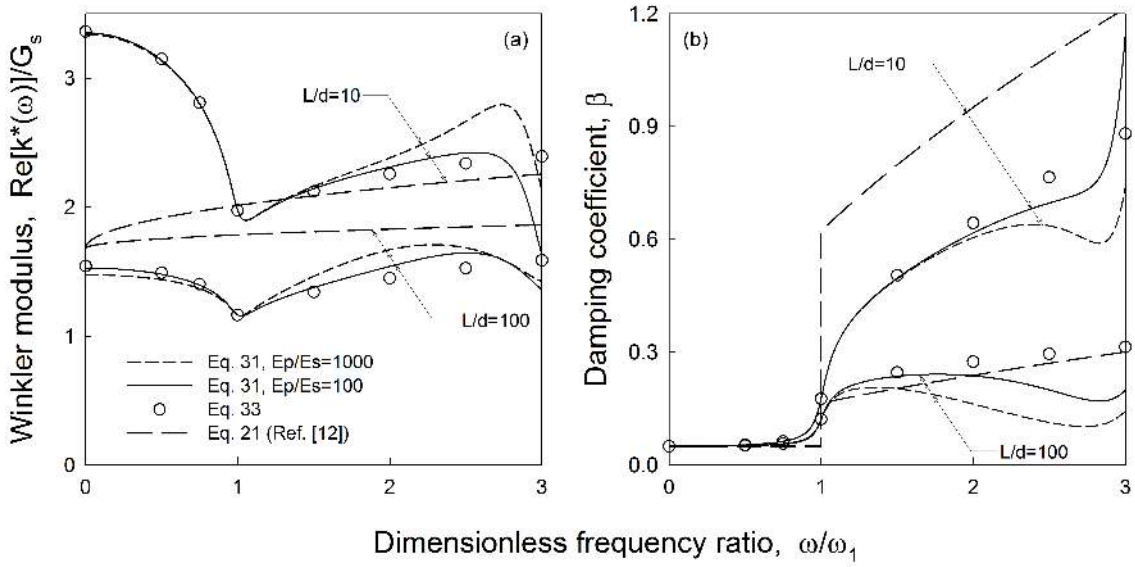

Figure 11. Comparison of average kinematic Winkler moduli predicted by various formulations; $\beta_s = 0.05$

6.1. Resonant conditions

Winkler modulus at resonance, $k(\omega_1)$, is further investigated in Figure 12. It is shown that soil material damping plays a major role in spring stiffness, the latter increasing with increasing material damping β_s. The actual $k(\omega_1)$ may be determined from the approximate expressions in Equations

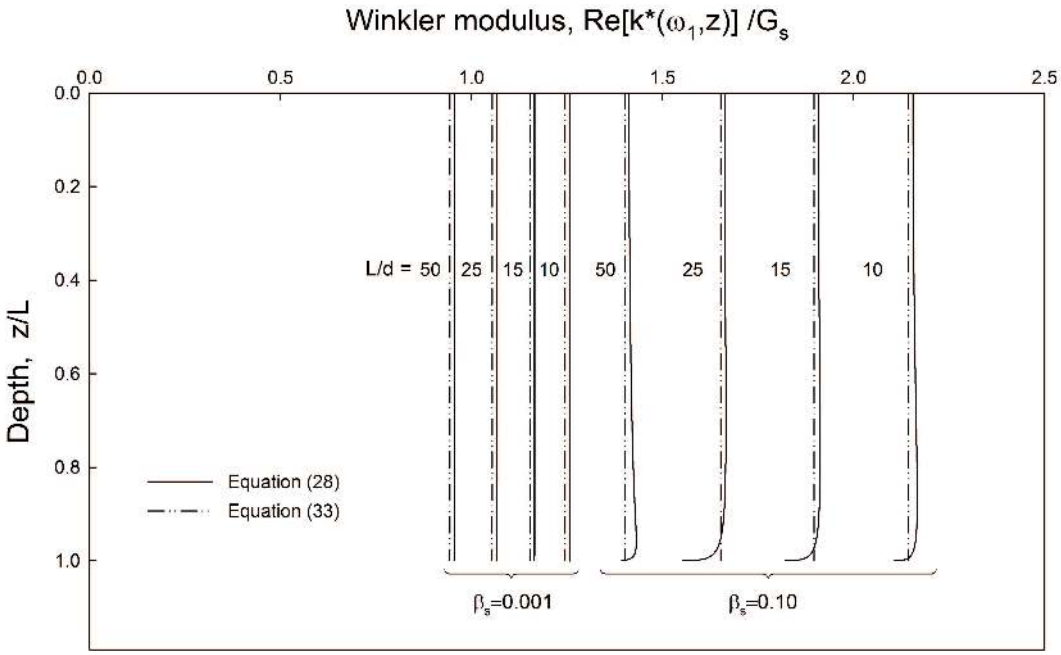

Figure 12. Variation of Winkler modulus with depth at resonant conditions ($\omega = \omega_1$) for different pile-soil configurations.

(33) and (35) for $a_0 = a_{cutoff}$, which do not encompass E_p/E_s and the spatial variable z. For low values of soil material damping, Equation (35) simplifies to

$$k^*(\omega_1) \;=\; \frac{2\,\pi\,G_s^*}{\ln 4 \;-\; \gamma \;-\; \ln\left[\eta_s \dfrac{\pi}{2}\dfrac{d}{L}\sqrt{2i\beta_s}\right]} \tag{36}$$

Note that for zero material damping β_s, the above expression yields zero spring stiffness which is in accordance with physics of the problem since the displacement of an undamped horizontal soil "slice"at resonance is infinite and thus its stiffness drops to zero.

Figure 12 shows that results obtained from the approximate expressions in Equations (33) and (35) can faithfully describe the behavior of k at first resonance for all pile-soil configurations examined. It should be noted that the depth-independent behavior is true only for dynamic springs, as the damping coefficient β varies with depth at resonance.

The variation of $k(\omega_1)$, computed from Equations (33) and (36), as function of the fundamental resonant frequency is depicted in Figure 13 for selected values of soil material damping. It is shown that resonant Winkler modulus increases with increasing resonant frequencies and soil material damping. The predictions of Equation (35) match almost perfectly those of Equation (33).

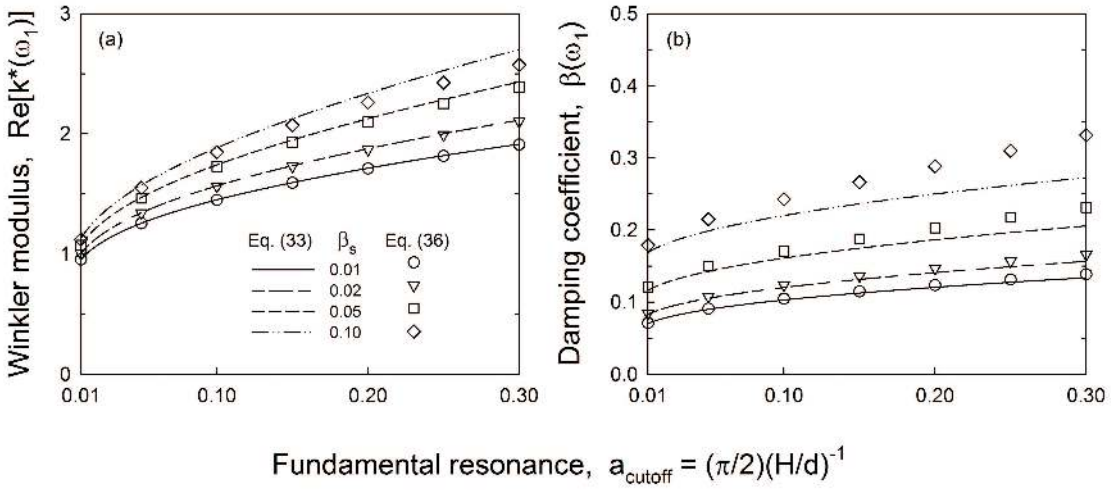

Figure 13. Variation of resonant Winkler moduli with level of resonant frequency.

The results discussed in Sections 5 and 6 clearly indicate the depth and frequency dependence of the equivalent distributed springs along the periphery of the pile, which is hard to model in the realm of simplified Winkler analyses, as the governing equations are challenging to solve in closed form. Nevertheless, in the frequency range of the most practical interest $0 \leq \omega \leq \omega_1$, the dependence of the distributed springs on depth is minor, which justifies the use of the average formulations in Equations (33) to (36).

7. HARMONIC AND TRANSIENT ANALYSES

The approximate expressions in Equations (33) to (36) can be employed in Winkler formulations to provide improved results over existing models. Results for the amplification factor $|\mathbf{A}|$ for a selected pile-soil configuration obtained from the proposed analysis and a Winkler model employing different expressions for modulus k, are plotted against excitation frequency in Figure 14(a). At resonance, the simplified frequency-dependent moduli in Equations (33) to (35) provide results that are in excellent agreement with the more rigorous elastodynamic model in Equations (17) and (26). On the contrary, the spring and dashpot coefficients in Equation (21) reported in Reference [12], lead to a deviation in pile head amplification on the order of 30% at first resonance. Outside resonance, however, kinematic response estimated from the simple formulae exhibit deviations over the finite-element results. Except from Equation (36) which employs a constant value pertaining to resonance, the performance of the various approaches is satisfactory.

Using frequency-independent moduli $k(\omega_1)$ and $\beta(\omega_1)$ captures well resonant conditions, yet leads to significant overestimation of the amplification factor at high frequencies, due to a profound underestimation of effective damping after first resonance, and thus should not be employed in harmonic analyses. Instead, resonant spring and dashpot moduli could be used in transient analyses as the overall response is governed by first resonance in the soil mass.

The successful performance of resonant moduli $k^*(\omega_1)$ is illustrated in Figure 15, where time histories of pile-head accelerations obtained from the proposed model and a Winkler model employing frequency-dependent Winkler moduli are compared. The bedrock motion is represented from two recorded motions with different frequency content, as shown in Figure 14(b). Despite the fact that all approaches seem to coincide, peak acceleration attains different values. In particular, expressions (33) and (35) lead to errors of less than 1% for Tolmezzo signal and less than $1‰$ for Koroni signal over the proposed model, whereas the simplest frequency-independent moduli in Equation (36) provide better performance over the existing frequency-dependent expressions in Equation (21) ([12]). However, a relevant difference in the performance of resonant Winkler moduli for the two signals is observed. This may be explained given that Koroni signal is characterized by a very narrow band of relevant frequencies located below the predominant frequency of the soil. In this range, the frequency-independent moduli provide satisfactory results (see Figure 14(a)). On the contrary, the predominant frequencies of Tolmezzo signal partially lie beyond the fundamental frequency of the soil, therefore expression (36) provides a less satisfactory performance in harmonic analyses.

8. CONCLUSIONS

A novel theoretical model was derived for the analysis of end-bearing piles embedded in a homogeneous soil stratum over a rigid base under vertically impinging seismic P waves. Within the framework of elastodynamic theory, a continuum wave solution was developed to quantify kinematic soil-pile interaction in terms of both stresses and displacements along the pile. The proposed model is approximate as it neglects equilibrium and displacement compatibility of soil

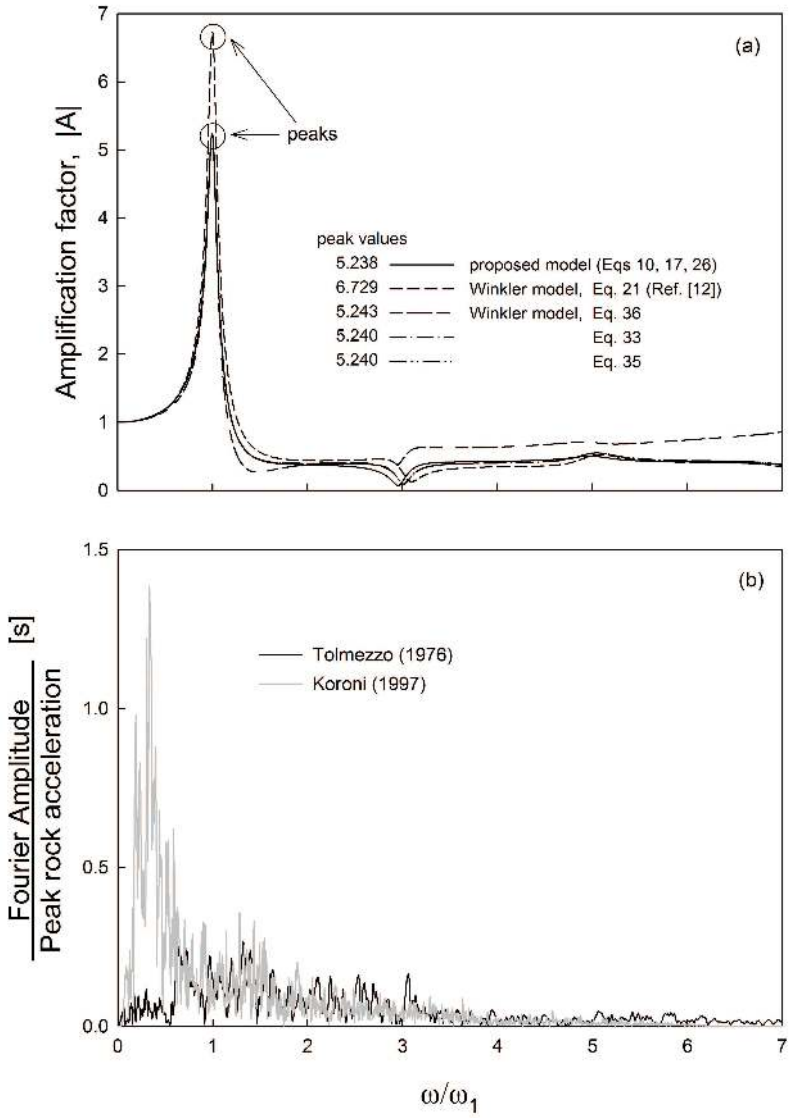

Figure 14. (a) Amplification factor A obtained from the proposed model and Winkler models for different selections of spring and dashpot coefficients (b) Fourier spectra of the rock motions employed; $L = 20\,m,\ d = 0.8\,m,\ E_p = 3 \times 10^7\,KPa,\ E_s = 10^4\,KPa,\ \nu_s = 0.4,\ \rho_s = 1.75\,Mg/m^3,\ \rho_p = 2.5\,Mg/m^3,\ \beta_s = 0.05.$

and pile in the direction perpendicular to loading, yet allows the solution to be obtained in closed form. The main conclusions of the study are:

1. Results for pile and soil displacements are in very good agreement with corresponding results obtained from rigorous FE solutions and offer a better representation of the problem over simplified Winkler models such as those discussed in Reference [12]. This confirms that the violations in equilibrium and in compatibility in the direction normal to loading are of minor importance for the specific problem. Similar conclusions have been reached in investigations of other related problems including those by Wood [37], Nogami & Novak [17] and Younan & Veletsos [26].

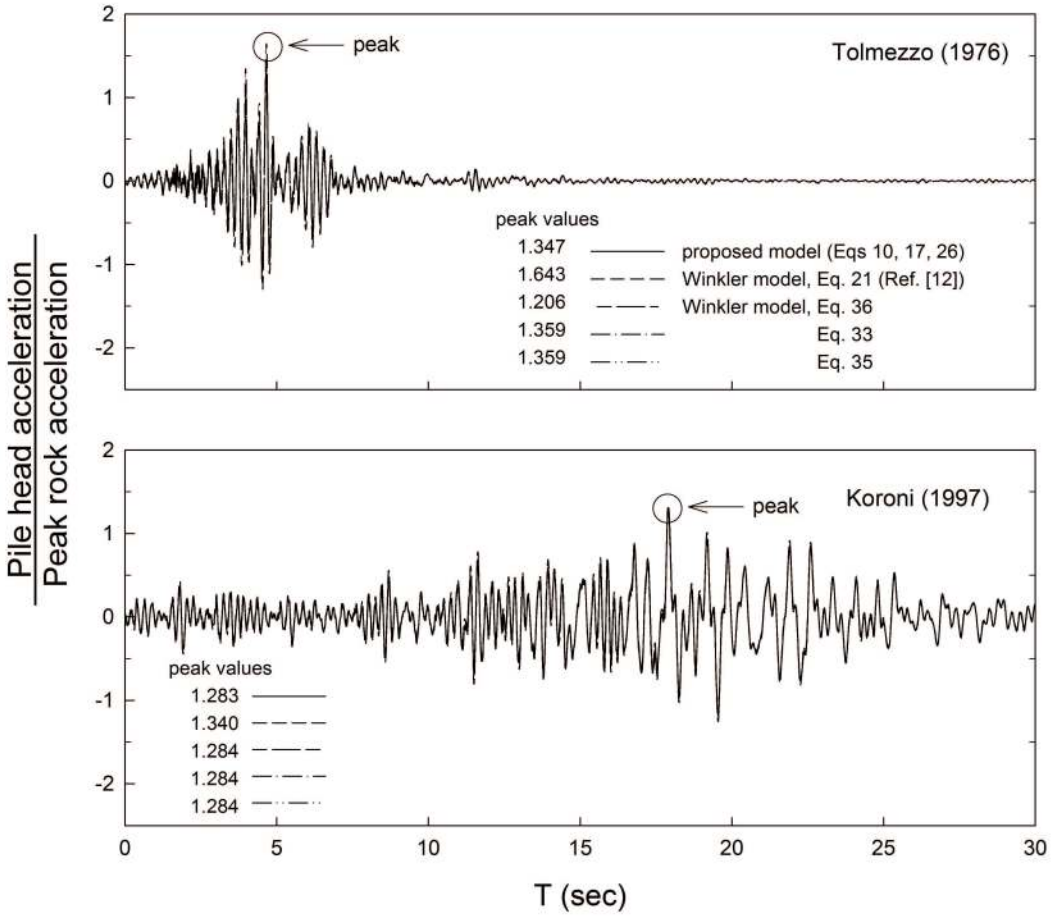

Figure 15. Time histories of pile-head acceleration obtained from the proposed model and Winkler models for different selections of spring and dashpot coefficients; $L = 20\,m$, $d = 0.8\,m$, $E_p = 3 \times 10^7\,KPa$, $E_s = 10^4\,KPa$, $\nu_s = 0.4$, $\rho_s = 1.75\,Mg/m^3$, $\rho_p = 2.5\,Mg/m^3$, $\beta_s = 0.05$.

2. The combined influence of pile-soil stiffness ratio E_p/E_s and pile slenderness L/d on kinematic response is described by a mechanical slenderness L_m (similar to dimensionless parameter λL in Winkler models). Pile-soil configurations with similar values of L_m, tend to respond in a similar manner.
3. Local minima of kinematic factor $|I_{\mathrm{v}}|$ occur at the natural frequencies of the soil layer, leading to an oscillatory behavior with increasing frequency. This wavy pattern is suppressed for long and/or soft piles having mechanical slenderness $(L/d)(E_p/E_s)^{-1/2}$ greater than approximately 2.
4. At high frequencies, $|I_{\mathrm{v}}|$, may be greater than unity for stiff piles, with the trend being more pronounced for higher values of soil material damping. However, this does not indicate an amplification of base motion at the pile head, since at such frequencies surface soil motion is deamplified over base motion. On the contrary, flexible piles experience $|I_{\mathrm{v}}|$ values lower than unity, yet they amplify base motion. Such an amplification, however, occurs only close to the first resonance of the soil layer.

5. Kinematic Winkler moduli along piles, like corresponding inertial moduli, are both frequency- and depth-dependent even in homogeneous soil. Nevertheless, kinematic Winkler moduli exhibit "mirror image" patterns compared to inertial moduli derived for piles subjected to axial harmonic loading at the top. At the fundamental resonant frequency of the soil layer kinematic Winkler k becomes essentially independent of depth, as in plane strain models.
6. The simplified depth-independent Winkler moduli in Equations (33) and (35) offer better approximations over existing formulas (Equation 21) employed in previous studies (Reference [12]).
7. Simplified expression in Equation (36) for Winkler moduli provide satisfactory performance for calculating pile head displacements. In transient analysis, the accuracy of this approximation increases when the frequency content of the input rock motion lies below the fundamental frequency of the soil layer.

It is fair to mention that the adoption of an elastic linear relation between stresses and displacements and the assumption of a perfectly bonded interface between soil and pile represent limitations of the model. Accordingly, some of the results reported in this work may require revision in presence of strong material nonlinearities induced by high-amplitude earthquake shaking.

ACKNOWLEDGEMENT

The research proposed in this paper was partially supported by the University of Patras through a Caratheodory Grant (#C.580). The authors are grateful for this support. The authors would like to thank the anonymous reviewer whose comments improved the quality of the original manuscript.

REFERENCES

1. Wolf JP. *Dynamic Soil-Structure Interaction*. Prentice-Hall. N.J., 1985.
2. Gazetas G & Mylonakis G. Seismic soil-structure interaction: New evidence and emerging issues. *Geotechnical earthquake engineering and soil dynamics* III, P. Dakoulas, M. K. Yegian, and R. D. Holtz, eds., Vol. II, ASCE, Reston, Va., 1998; 1119-1174.
3. Maiorano RMS, de Sanctis L, Aversa S, Mandolini A. Kinematic response analysis of piled foundations under seismic excitation. *Canadian Geotechnical Journal* 2009; **46**(5):571-584.
4. Zarzalejos JM, Aznrez JJ, Padrn LA, Maeso O. *Influence of type and angle of incident waves on seismic pile bending at cap level* Second International Conference on Performance-Based Design in Earthquake Geotechnical Engineering, Taormina, Sicily, 28-30 May 2012; SESSION 11.b.
5. de Sanctis L, Maiorano RMS, Aversa S. A method for assessing kinematic bending moments at the pile head. *Earthquake Engineering & Structural Dynamics* 2010; **39**(10):1133−1154.

6. Di Laora R, Mylonakis G, Mandolini A. Pile-head kinematic bending in layered soil. *Earthquake Engineering & Structural Dynamics* 2012; DOI:10.1002/eqe.2201.
7. Di Laora R, Mandolini A, Mylonakis G. Insight on kinematic bending of flexible piles in layered soil. *Soil Dynamics & Earthquake Engineering* 2012; **43**:309−322. http://dx.doi.org/10.1016/j.soildyn.2012.06.020
8. Kaynia AM, Kausel E. *Dynamic stiffness and seismic response of pile groups*. Research Report R82-03, Department of Civil Engineering, MIT: Cambridge, Mass, 1982.
9. Di Laora R. *Seismic soil-structure interaction for pile supported systems*. PhD Thesis University of Napoli, "Federico II", 2009.
10. Barghouthi AF. *Pile response to seismic waves*. PhD thesis, Univ. of Wisconsin, Madison, Wis, 1984.
11. Ji F, Pak RYS. Scattering of vertically incident P waves by an embedded pile. *Soil Dynamics & Earthquake Engineering* 1996; 15:211-222.
12. Mylonakis G, Gazetas G. Kinematic pile response to vertical P-wave seismic excitation. *Journal of Geotechnical and Geoenvironmental Engineering* (ASCE) 2002; **128**(10):860-867.
13. Papazoglou AJ, Elnashai AS. Analytical and field evidence of the damaging effect of vertical earthquake ground motion. *Earthquake Engineering & Structural Dynamics* 1998; **25**(10):1109-1137.
14. Hetenyi M. *Beams on Elastic Foundations*. Ann Arbor: The University of Michigan Press, 1946.
15. Scott RF. *Foundation Analysis*. Englewood Cliffs, NJ. Prentice-Hall, 1981.
16. Tajimi H. Dynamic analysis of a structure embedded in an elastic stratum. *Proc. 4th World Conference on Earthquake Engineering* 1969, Santiago III(A-6); 53-69.
17. Nogami T, Novak M. Soil-pile interaction in vertical vibration. *Earthquake Engineering & Structural Dynamics* 1976; **4**(3):277-293.
18. Saitoh M. Fixed-head pile bending by kinematic interaction and criteria for its minimization at optimal pile radius. *Journal of Geotechnical and Geoenvironmental Engineering* (ASCE) 2005; **131**(10):1243-1251.
19. Anoyatis G, Mylonakis G. Dynamic Winkler modulus for axially loaded piles. *Géotechnique* 2012. **62**(6):521-536.
20. Baranov VA. On the calculation of an embedded foundation. *Vorposy Dinamiki i Prognostic* (Polytechnical Institute of Riga, Latvia) 1967; (14):195-209, (in Russian).
21. Novak M. Dynamic stiffness and damping of piles. *Canadian Geotechnical Journal* 1974; **11**(4):574-598.
22. Graff KF. *Wave motions in elastic solids*. Oxford: Oxford University Press, 1975.
23. Mylonakis G. Winkler modulus for axially-loaded piles. *Géotechnique* 2001; **51**(5):455-461.
24. Anoyatis G. *Elastodynamic analysis of piles for inertial and kinematic loading*. MSc Thesis, University of Patras, Rio, Greece (in Greek), 2009.
25. Anoyatis G, Mylonakis G. Novel Tajimi models for static and dynamic soil-pile interaction. *8th International Conference on Structural Dynamics, EURODYN 2011*, 4-6 July, Leuven, Belgium.
26. Younan A, Veletsos A. Dynamic response of flexible retaining walls. *Earthquake Engineering & Structural Dynamics* 2000; **29**(12):1815−1844.

27. Roesset JM. Soil amplification of earthquakes. *Numerical Methods in Geotechnical Engineering*, (Eds. Desai CS and Christian JT) McGraw-Hill, New York, 1977.

28. Kramer SL. *Geotechnical Earthquake Engineering*. Prentice-Hall: NY, 1996.

29. ANSYS Inc. *ANSYS Theory Reference 10.0*. Canonsburg, Pennsylvania, US. 2005.

30. Rosset JM. Stiffness and damping coefficients of foundations. *Proc. ASCE Geotechnical Engineering Division National Convention*, October 30, 1980; 130.

31. Gazetas G, Dobry R. Horizontal response of piles in layered soils. *Journal of Geotechnical Engineering* 1984; **110**(1):20-40.

32. Mylonakis G. Elastodynamic model for large-diameter end-bearing shafts. *Soils and Foundations* 2001; **41**(3):31-44.

33. Anoyatis G, Di Laora R, Mandolini A, Mylonakis G. Kinematic response of single piles for different boundary conditions: Analytical solutions and normalization schemes. *Soil Dynamics & Earthquake Engineering* 2013; **44**:183−195.

34. Prieto F, Lourenco PB, Oliveira CS. Impulsive Dirac-delta forces in the rocking motion. *Earthquake Engineering & Structural Dynamics* 2004; **33**(7):839−857.

35. Veletsos A, Ventura C. Dynamic analysis of structures by the DFT method. *Journal of Structural Engineering, ASCE* 1985; **111**(12):2625−2642.

36. Nakamura N. A practical method to transform frequency dependent impedance to time domain. *Earthquake Engineering & Structural Dynamics* 2006; **35**(2):217−231.

37. Wood JH. *Earthquake-induced Soil Pressures on Structures.* PhD Thesis, CaltechEERL:1973.EERL-73-05.